Electronic Supplementary Information

Lattice Doping and NiO Synergistic Decoration for Enhanced CO_2 Electrolysis in Solid Oxide Electrolysis Cell

Maoyu Kang,[a] Shu Xiao,[a] Qiran Zhang,[a] Jinhuang Cai,[a] Dunkui Li,[a] Chang-An Zhou,*[a] Hongjiao Li,[a] Chao Wang,[a] Lei Song,[a] Kui Ma,*[a] and Hairong Yue [a,b,c]

a. *Low-Carbon Technology and Chemical Reaction Engineering Laboratory, School of Chemical Engineering, Sichuan University, Chengdu 610065, China.*
b. *Institute of New Energy and Low-Carbon Technology, Sichuan University, Chengdu 610207, China.*
c. *Coal Mining Research Institute, China Coal Technology and Engineering Group, Beijing 100013, China*

*Corresponding author: kuima@scu.edu.cn, TEL/FAX: (+86) 28-85465318

Experimental section

1. Material synthesis

The NiO/Ni-$Sm_{0.2}Ce_{0.8}O_{2-\delta}$-x cathode powders were synthesized via the sol-gel method, where x (x = 0.100, 0.125, 0.150, and 0.175) represents the molar ratio of Ni species introduced into the $Sm_{0.2}Ce_{0.8}O_{2-\delta}$ (SDC). Stoichiometric amounts of $Sm(NO_3)_3 \cdot 6H_2O$ and $Ce(NO_3)_3 \cdot 6H_2O$ were dissolved in an appropriate volume of deionized water, with citric acid and polyvinyl alcohol added in specified proportions. The solution was continuously heated and stirred in a 150 °C oil bath, then dried to obtain the precursor powders. The powders were ground and calcined at 1000 °C for 5 h in air to obtain pristine SDC powders. The NiO/Ni-SDC-x samples were prepared according to the same procedure with additional $Ni(NO_3)_2 \cdot 6H_2O$. And the molar ratio of metal nitrates was Ni:Sm:Ce = x:(0.2-x):0.8. Additionally $La_{0.6}Sr_{0.4}Co_{0.2}Fe_{0.8}O_{3-\delta}$ (LSCF) powders were synthesized using the same method. LSCF powders and SDC

powders were mixed and ground at a weight ratio of 3:2 to obtain the LSCF-SDC anode composite powders.

2. Cell fabrication

An electrolyte cell with an NiO/Ni-SDC|SDC|LSGM|LSCF-SDC structure was prepared, where SDC serves as a barrier layer to ensure electrode-electrolyte bonding. LSGM electrolyte was prepared via tape-casting technique, with a thickness of approximately 210 μm and a diameter of 15 mm. Electrode slurry was prepared by mixing electrode powders with organic binder at a weight ratio of 5:3. The slurry was screen-printed onto both sides of the electrolyte and sintered at 1150 °C for 2 h to form electrodes. Silver paste was coated onto the electrodes as current collectors.

3. Physicochemical characterization

X-ray diffraction (XRD) testing was performed at room temperature using an XRD instrument (Shimadzu, Japan, XRD6100) equipped with a Cu Kα target (λ=1.5418 Å). Scanning electron microscopy (SEM) images were collected on a ZEISS Sigma 300 instrument. Transmission electron microscopy (TEM) images were obtained using a JEOL JEM-F200 instrument. Raman spectra were acquired using a Horiba LabRAM HR Evolution Raman spectrometer (532 nm). Powder X-ray photoelectron spectroscopy (XPS) analysis was performed using a Thermo Scientific K-Alpha spectrometer, with binding energy calibrated using C 1s (284.8 eV). Carbon dioxide temperature-programmed desorption (CO_2-TPD) testing of the powders was performed on a Micromeritics Autochem III 2930 instrument. Electron paramagnetic resonance (EPR) testing was conducted on a Bruker EMX Plus spectrometer.

4. Electrochemical measurements

The electrochemical performance of the cell was tested on an alumina tube placed inside a tubular furnace, with the gas chamber sealed using a high-temperature fused glass ring. A 95% CO_2-5% N_2 gas flowed toward the cathode at a rate of 40 ml min^{-1}, while the anode side was exposed to static ambient air. Electrochemical testing was conducted within the 700-800 °C range. Electrochemical performance was

evaluated using current density-voltage (J-V), electrochemical impedance spectroscopy (EIS) measurements and constant potential on a Donghua 7002A electrochemical workstation. The produced gas CO was analyzed by gas chromatography (GC2060) to calculate Faraday efficiency. J-V curves were measured at a scan rate of 10 mV s^{-1} within the 0-1.6 V range. EIS was performed at an amplitude of 10 mV across the 0.01–10^5 Hz frequency range. The obtained EIS data were analyzed using the relaxation time distribution (DRT) tool and fitted with Zview software.

5. Density functional theory (DFT) calculation

DFT calculations were conducted using the Vienna ab initio simulation package (VASP 6.0).[1] The calculations employed Projector Augmented Wave (PAW) potentials to describe ionic cores[2] and Perdew-Burke-Ernzerhof (PBE) exchange-correlation functional[3] with Hubbard U corrections[4] for correct electronic structures (U–J values were 6.0 eV for Ce and Sm, and 5.96 eV for Ni). The thermodynamically most favorable one is used for data analysis. The cut-off kinetic energy of 450 eV and the convergence criteria of 10^{-6} eV was used for all calculations. A geometry optimization scheme using a conjugate gradient algorithm was used to optimize the atomic positions, cell shapes, and volumes until the maximum force on any atom was less than 0.02 eV·$Å^{-1}$. The Brillouin zone of all systems was sampled using a Monkhorst-Pack grid.[5] The Fermi energy levels were smoothed using Gaussian smearing with a Gaussian width of 0.02 eV.

Figures and Tables

Table S1 Proportion of O species in SDC and NiO/Ni-SDC-x sample obtained by XPS analysis.

Sample	Relative content (%)		
	O_L	O_R	O_S
SDC	44.23	17.89	37.88
NiO/Ni-SDC-0.100	40.52	23.64	35.84
NiO/Ni-SDC-0.125	37.48	28.31	34.21
NiO/Ni-SDC-0.150	29.09	33.83	37.08
NiO/Ni-SDC-0.175	24.54	38.71	36.75

Table S2 Equivalent circuit fitting results of SDC and NiO/Ni-SDC-0.150 cell at 800 °C and 1.4 V.

Cell	Ohmic resistance (Ω cm^2)	Polarizational resistance (Ω cm^2)			
	R_o	R_{p1}	R_{p2}	R_{p3}	R_p (total)
SDC	0.144	0.072	0.082	0.146	0.300
NiO/Ni-SDC-0.150	0.153	0.054	0.047	0.076	0.177

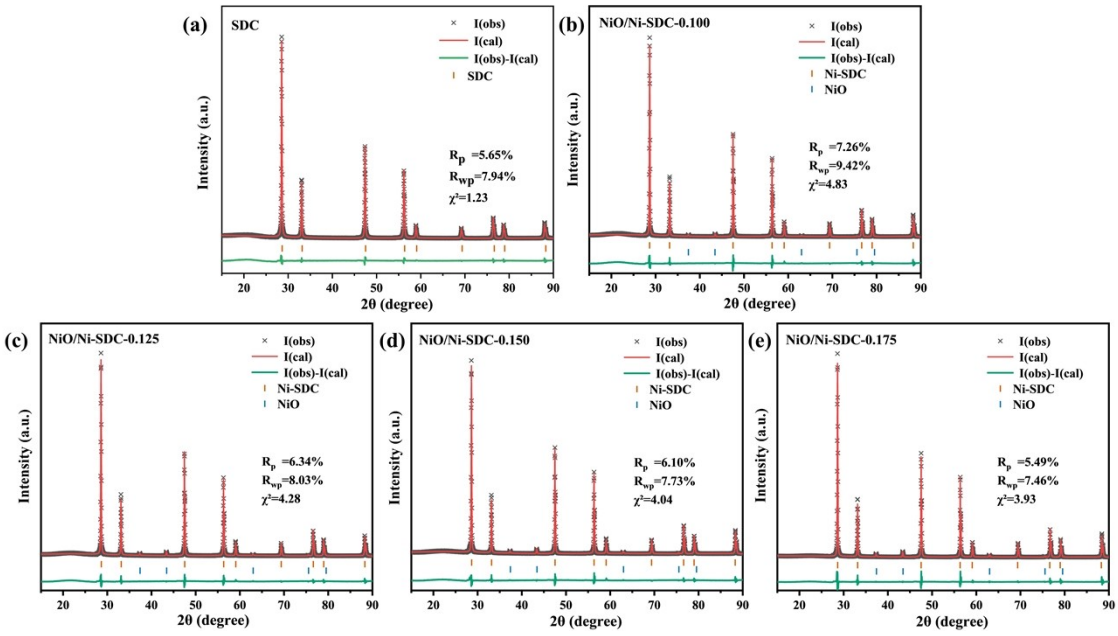

Fig. S1 Rietveld refinement profiles of (a) SDC, (b) NiO/Ni-SDC-0.100, (c) NiO/Ni-SDC-0.125, (d) NiO/Ni-SDC-0.150, and (e) NiO/Ni-SDC-0.175.

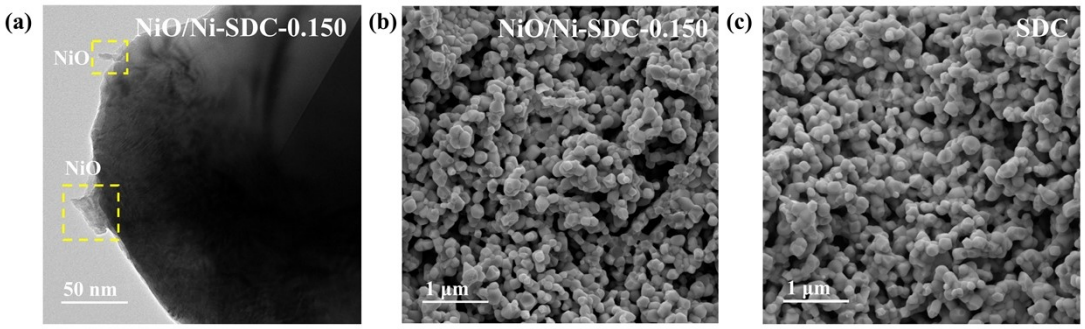

Fig. S2 (a) TEM characterization of NiO/Ni-SDC-0.150 powders. SEM characterization of (b) NiO/Ni-SDC-0.150 and (c) SDC powders.

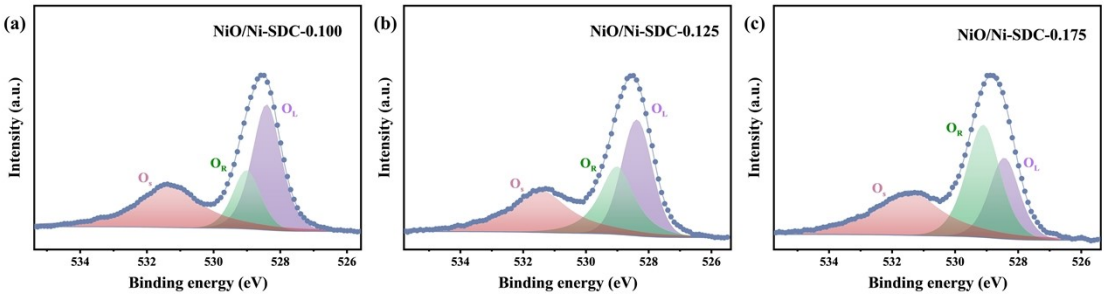

Fig. S3 XPS spectra of O 1s for (a) NiO/Ni-SDC-0.100, (b) NiO/Ni-SDC-0.125 and (c) NiO/Ni-SDC-0.175.

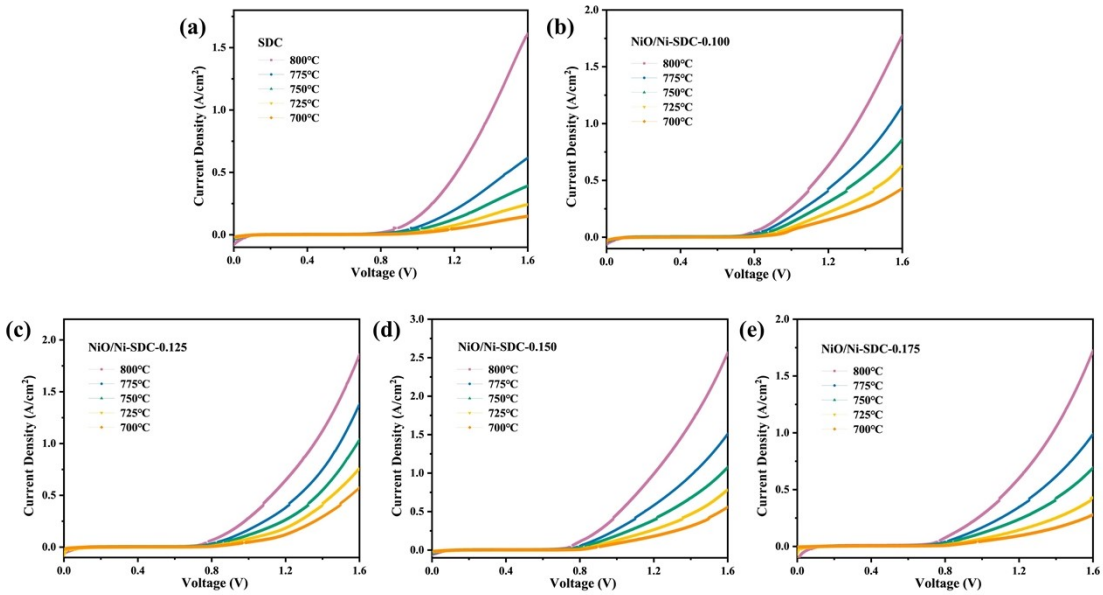

Fig. S4 J-V curves at 700-800 °C of (a) SDC, (b) NiO/Ni-SDC-0.100, (c) NiO/Ni-SDC-0.125, (d) NiO/Ni-SDC-0.150 and (e) NiO/Ni-SDC-0.175.

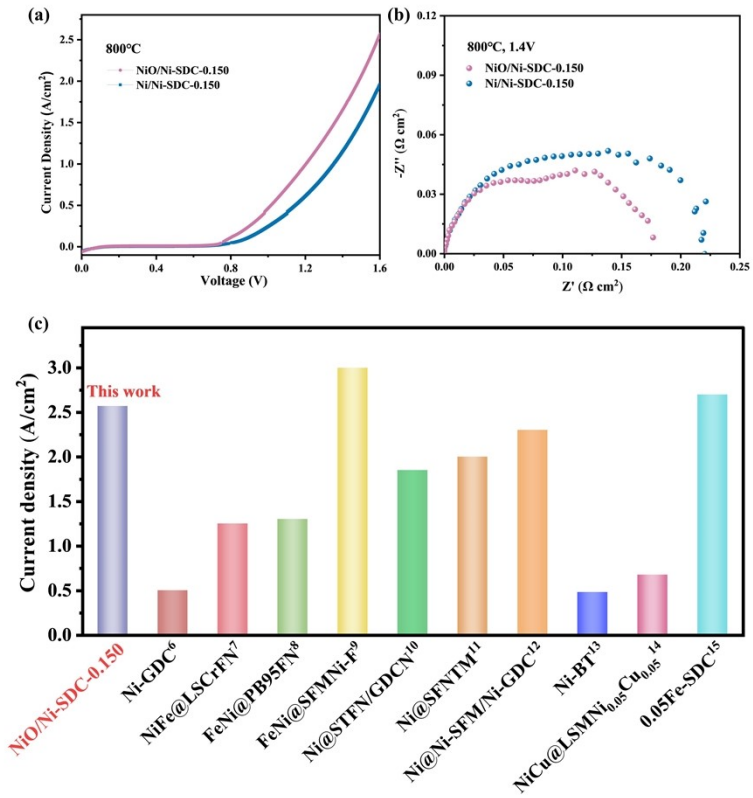

Fig. S5 (a) J-V curves at 800 °C of NiO/Ni-SDC-0.150 and reduced NiO/Ni-SDC-0.150. (b) EIS spectra recorded at 800 °C, 1.4 V of NiO/Ni-SDC-0.150 and reduced NiO/Ni-SDC-0.150. (c) Comparison of the CO_2 electrolysis performance with other advance electrodes[6–15] testing at 800 °C, 1.6 V.

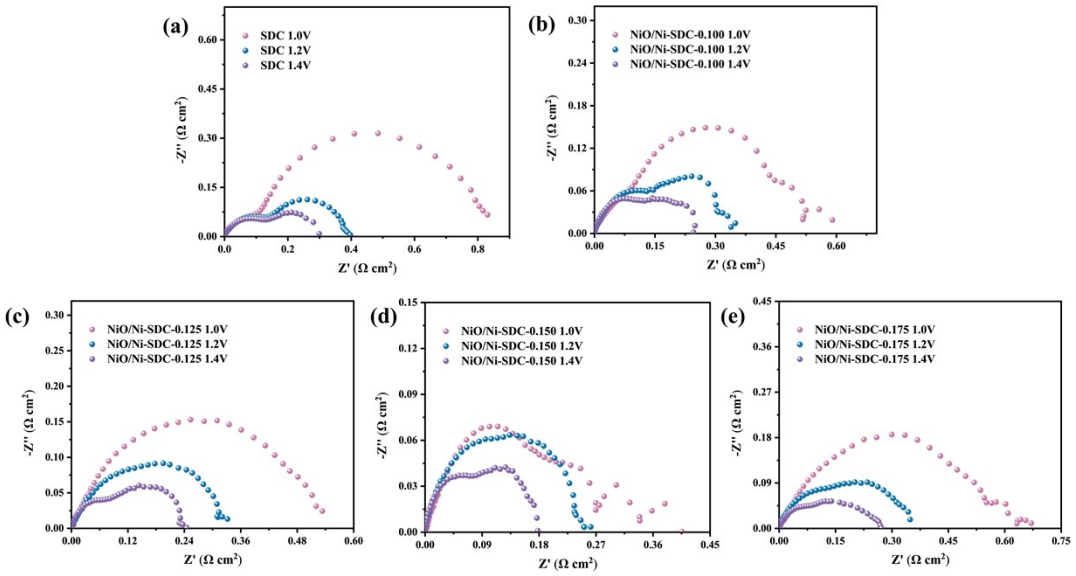

Fig. S6 EIS spectra recorded at 800 °C under voltages of 1.0 V, 1.2 V, and 1.4 V of (a) SDC, (b) NiO/Ni-SDC-0.100, (c) NiO/Ni-SDC-0.125, (d) NiO/Ni-SDC-0.150 and (e) NiO/Ni-SDC-0.175.

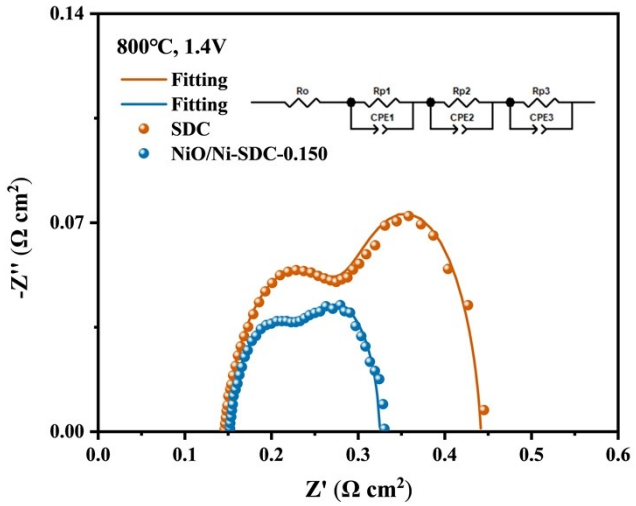

Fig. S7 CNLS-fitted EIS spectra of SDC and NiO/Ni-SDC-0.150 cell at 800 °C and 1.4 V.

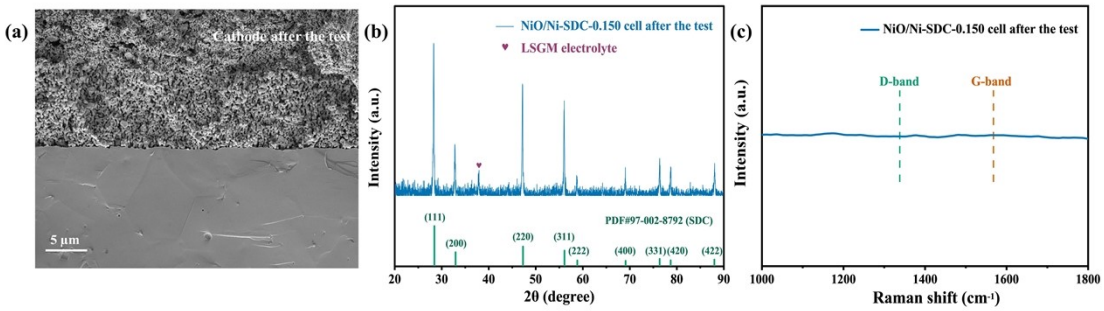

Fig. S8 (a) SEM characterization of the cross section of NiO/Ni-SDC-0.150 cathode/electrolyte structure after the long-term stability test. (b) XRD patterns of the NiO/Ni-SDC-0.150 cell after the test. (c) Raman spectra after long-term stability test.

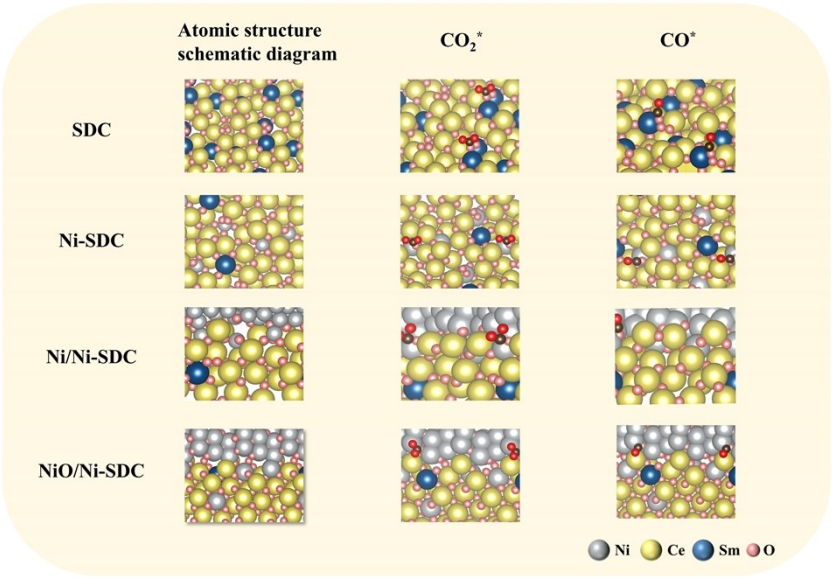

Fig. S9 Atomic structure model of SDC, Ni-SDC, Ni/Ni-SDC and NiO/Ni-SDC.

For the DFT calculations, the following structural models were constructed: the pristine SDC; SDC doped with nickel into the lattice (Ni-SDC); and SDC with Ni species partially incorporated into the SDC lattice and partially distributed on the surface as NiO (NiO/Ni-SDC, this work), part of the Ni species enters the SDC lattice, while the others are distributed as the Ni metal on the surface (Ni/Ni-SDC).

Reference

1 G. Kresse and J. Furthmüller, *Phys. Rev. B*, 1996, **54**, 11169-11186.

2 G. Kresse and D. Joubert, *Phys. Rev. B*, 1999, **59**, 1758-1775.

3 J. P. Perdew, K. Burke and M. Ernzerhof, *Phys. Rev. Lett.*, 1996, **77**, 3865-3868.

4 A. J. Cohen, P. Mori-Sánchez and W. Yang, *Science*, 2008, **321**, 792-794.

5 D. J. Chadi, *Phys. Rev. B*, 1977, **16,** 1746-1747.

6 A. Abu Hajer, D. A. Daramola and J. P. Trembly, *Electrochimica Acta*, 2024, **485**, 144052.

7 M. Wang, N. Li, Q. Shen, Z. Zhan and C. Chen, *Sustainable Energy Fuels*, 2022, **6**, 2038-2044.

8 X. Wang, H. Hu, C. Xie, Y. Wang, H. Li and X. Ding, *J. Mater. Chem. A*, 2024, **12**, 11701-11709.

9 S. Zhang, Y. Jiang, H. Han, Y. Li and C. Xia, *ACS Appl. Mater. Interfaces*, 2022, **14**, 28854-28864.

10 T. Wang, N. Sun, R. Wang, D. Dong, T. Wei and Z. Wang, *Journal of Power Sources*, 2025, **626**, 235821.

11 S. Zhen, L. Zhang, C. Xu, D. Zhang, Q. Yi, W. Sun and K. Sun, *Front. Chem.*, 2022, **10**, 1027713.

12 F. Hu, Y. Ling, S. Fang, L. Sui, H. Xiao, Y. Huang, S. Wang, B. He and L. Zhao, *Applied Catalysis B: Environmental*, 2023, **337**, 122968.

13 D. Aini, M.-S. Lin, R. Ismail, A. Parkash, Y.-L. He, P.-C. Ma and A. Kadier, *International Journal of Hydrogen Energy*, 2025, **191**, 152250.

14 X. Gao, L. Ye and K. Xie, *Fuel*, 2024, **371**, 131959.

15 L. Zhang, Y. Jiang, K. Zhu, N. Shi, Z. U. Rehman, R. Peng and C. Xia, *Small Methods*, 2024, **8**, 2301686.